

Adaptive Variable Stiffness Particle Phalange for Robust and Durable Robotic Grasping

Jianshu Zhou,¹ Yonghua Chen,¹ Yong Hu,² Zheng Wang,¹ Yunquan Li,¹ Guoying Gu,³ and Yunhui Liu⁴

Abstract

Grasping is an important characteristic of robots in interacting with humans and the environment. Due to the inherent compliance of soft grippers, they can easily adapt to novel objects and operate safely in a human-centered environment. However, soft hands suffer from poor grasping robustness and operation durability, especially for heavy objects or objects with sharp spikes, mainly due to their fragile material and low structural stiffness of the soft actuators. Thus, the widespread use of soft hands in daily applications is still limited. Existing works have shown a promising direction to enhance grasping performance by solving the contradiction between inherent compliance/adaptability and loading capacity. It is known that the stiffness of the robotic phalange is highly related to the performance of robotic hands. In this article, we propose a novel variable stiffness particle phalange, called VSPP here. The proposed VSPP exhibits variable stiffness characteristics without the need for dedicated actuation by utilizing passive particle jamming resulted from forces in interacting with the environment. The VSPP can cooperate with any kind of actuators, soft or rigid, to function as a compliant and robust robotic hand. A prototype robotic hand based on VSPP could maintain reliable grasping even when pierced by sharp objects such as a needle, a cactus, and a durian. This durability is effective both in air and underwater, thus presents new possibilities for the soft robotic hand to work in a harsh environment. The inherent multidirectional compliance of the VSPP makes safety in human/robot interaction guaranteed. The design and modeling presented in this research will provide useful guidance in VSPP applications. A prototype gripper, VSPP-3, composed of three 2-segments VSPP fingers and pneumatic joints, has been built for demonstrations in reliable and robust grasping of daily objects. The sample grasping has shown that the proposed VSPP has great potential for a robust and durable soft robotic hand or gripper design.

Keywords: soft grippers, variable stiffness, grasping robustness, grasping durability, passive particle jamming

Introduction

WITH THE RAPIDLY SPREADING APPLICATIONS of robots in our daily life, human-centered robotic systems are increasingly attracting the interest of researchers and engineers. Unlike traditional robots demanding high precision and rigidity in industrial applications, compliance is one of the critical considerations for human-centered robots to provide safe human/robot interaction.

Soft robotics, as a promising candidate to build safe human-centered robots, is rapidly progressing in recent years.^{1,2} Robotic hand/gripper is at the forefront of a robot in interacting with the

environment and humans.^{3,4} Compared with traditional rigid robotic hands actuated by motors, cables, and linear actuators, a soft hand exhibits distinctive compliance for both adaptable grasping and secure human/robot interaction. The Young's modulus of constructing material for soft hand is close to human beings and natural living things, which enables soft robot hands highly effective and safe in mimicking natural grasping.⁵

A lot of achievements on soft robot hands have been reported in recent decades. A recent tendency, focusing more on the actuation mechanisms/robotic joints, can be found in existing work.^{1,6} Among which, there are soft hands based on PneuNet or fiber-reinforced pneumatic actuators,^{7,8}

Departments of ¹Mechanical Engineering and ²Orthopaedics and Traumatology, The University of Hong Kong, Hong Kong, Hong Kong.
³Soft Robotics and Biodesign Lab, Robotics Institute, School of Mechanical Engineering, Shanghai Jiao Tong University, Shanghai, China.

⁴Department of Mechanical and Automation Engineering, The Chinese University of Hong Kong, Hong Kong, Hong Kong.

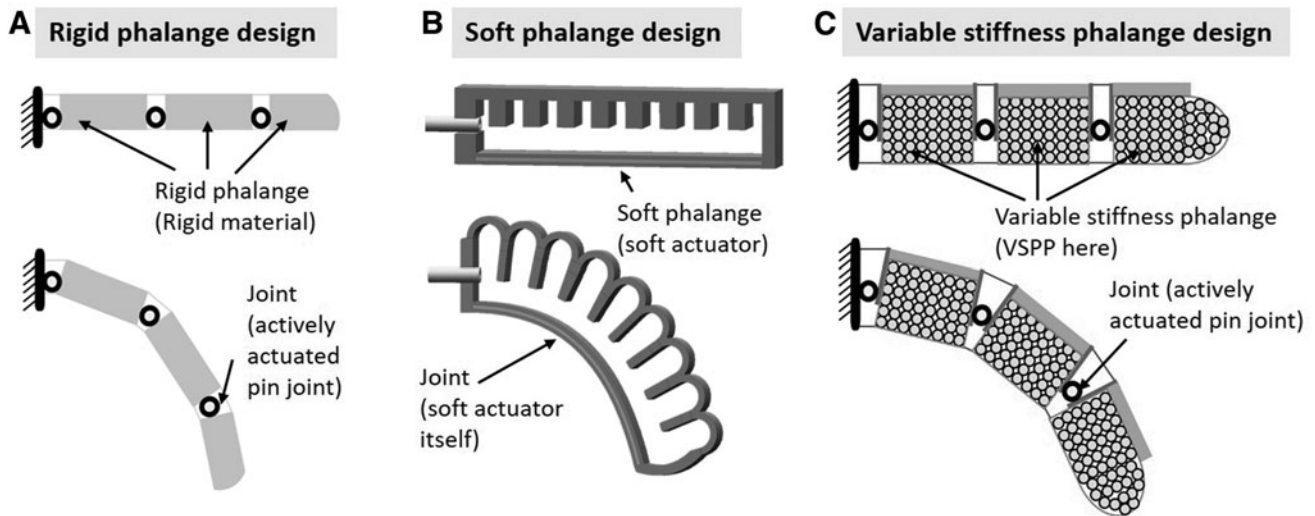


FIG. 1. Comparison of different phalange stiffness designs. (A) Rigid phalange-based robotic finger with pin joint kinematics. (B) Soft phalange-based robotic finger with PneuNet structure. (C) VSPP-based robotic finger with pin joint kinematics. VSPP, variable stiffness particle phalange.

cable-driven approach,^{9,10} shape memory alloy (SMA)-driven approach,¹¹ shape memory polymer (SMP)-driven approach,^{12,13} particle jamming approach,^{14,15} electroadhesive approach,¹⁶ and dielectric elastomer technology.^{17,18} The merits and drawbacks of existing soft hands are both conspicuous.

On the positive side, inherent compliance enables the soft hand to have extraordinary adaptability to unstructured environments, reliable safety for human/robot interaction, and simple structure with excellent affordability. On the contrary, the soft actuator also induces challenges such as poor operation durability and weak grasping robustness, especially in handling relatively heavy or spiky objects. This hampers further applications of soft robot hands.

Existing works have shown that good grasping performance needs a proper compromise between compliance/adaptability and load capacity.^{10,12–14,19–24} Rigid phalanges cooperated with powerful joints in traditional robotic hands ensure a large load capacity, whereas soft fingers in a soft robotic hand provide the grasping compliance/adaptability. The proposed variable particle stiffness phalange is a compromise between soft and rigid because of its variable stiffness feature.

Following this direction, the variable stiffness structure is a promising candidate to achieve the abovementioned performance.²⁵ Two main categories of variable stiffness mechanisms were reported. One type is active variable stiffness approaches such as active actuator impedance control.²⁶ The other type, semiactive methods, is by using the structural or material feature to realize variable stiffness. For example, there are semiactive approaches using a pneumatic variation,²⁷

particle jamming,^{14,19} electrorheological or magnetorheological material,^{28,29} SMA or SMP,^{13,23,30} low melting point alloys,³¹ and conductive elastomers.³² Among these, passive particle jamming, reported previously, used to strengthen the pneumatic soft actuators, is simpler in the mechanism.¹⁴ Here we further develop the passive particle jamming mechanism into a phalange unit as it can meet the requirement of variable stiffness of a phalange: low stiffness under small contact force and high stiffness under large contact force.

The structural comparison of the proposed variable stiffness particle phalange (VSPP) with those rigid grippers and soft finger is depicted in Figure 1. As depicted in Figure 1A, a traditional rigid finger is usually made of rigid phalanges/links. Connecting these rigid phalanges by joints in the desired order, we can build a rigid robotic hand with the anticipated kinematic mechanism.³³ The extreme to rigid fingers is the soft robotic finger as shown in Figure 1B, which is soft with continuous deformation.³⁴ The proposed VSPP finger shown in Figure 1C provides a compromise between those rigid and soft fingers. Each VSPP is made by a package of particles packed into an elastic membrane, which can be made by silicone rubber, three-dimensional (3D)-printed soft elastic material, or elastic fabrics.

We compared the influence of different phalange designs on the robotic hand performance, as depicted in Table 1. The proposed that VSPP can bridge the gap between the rigid and soft robotic fingers, and thus, it may have the combined merits of the other two types of robotic fingers. With the variable stiffness feature, VSPP-based robotic fingers can adjust their stiffness passively depending on the interaction force. Under small interaction force, VSPP fingers exhibit low stiffness and perform similarly to a soft hand; under large

TABLE 1. THE INFLUENCE OF DIFFERENT PHALANGE STIFFNESSES ON HAND PERFORMANCE

	<i>Rigid phalange gripper</i>	<i>Soft phalange gripper</i>	<i>Variable stiffness phalange gripper</i>
Phalange stiffness	Constant high stiffness	Constant low stiffness	Variable stiffness depending on the interaction force
Hand performance	(1) Robust (2) Durable	(1) Compliant (2) Safe	(1) Robust, (2) Durable (3) Complaint, (4) Safe

interaction force, the VSPP fingers will increase their stiffness because of passive jamming, which helps to enhance the grasping payload. The particle stiffness is mainly adaptive to contact forces in interaction with objects. At the same time, the VSPP structural stiffness is also enhanced after the passive jamming caused by force interaction. This is further described in the following sections.

As a VSPP only functions as a link of a robotic finger, the VSPP can cooperate with any kind of actuators, both rigid and soft, thus providing excellent design versatility. Furthermore, because the VSPP itself is separated from the actuation part, its failure will not affect the actuation system. As a result, VSPP-based fingers can be subjected to a very harsh environment, even objects with needle-sharp features. VSPP-based fingers have no need for seals as they do not rely on air/vacuum for their variable stiffness adjustment. Thus, they are still functional even when punctured. This puncture sustainability keeps effective even in underwater conditions. This excellent durability is not subject to change of temperature (as long as materials do not degrade), pressure, and electrical and magnetic field. Thus, the VSPP-based robotic hands can be applied to more cases where processing durability is required, or a new application context in a harsh environment such as grasping brambly creatures in the deep sea.

The contribution of this article can be highlighted in three major perspectives.

- (1) First, we proposed a novel VSPP for variable stiffness robotic finger design. The VSPP exhibits good compliance similar to soft robots under a small interaction force and provides large rigidity similar to rigid robots under a larger interaction force. This variable stiffness feature enables VSPP to be a promising candidate to solve the compromise between loading capacity and compliance/adaptability in robotic grasping.
- (2) Second, the design, fabrication, and modeling of VSPP are discussed in detail. The versatile fabrication and assembly approaches illustrated in the article provide clear guidance to replicate VSPP into customizable applications. The models induced in the article explain the passive jamming mechanisms of VSPP and the stiffness enhancement of the VSPP. All of these provide both a theoretic model and a specific reference to apply VSPP into more soft robotic applications.
- (3) Third, the effective grasping of the VSPP-3 gripper toward various objects, including a prickly cactus, a pineapple, and a heavy and sharp spiky durian, is presented. In the experimental grasping operations, the VSPP-based gripper has shown great load capability and adaptability. Even when pierced by sharp objects, the VSPP fingers were still effective. This has demonstrated that the proposed VSPP gripper could work in harsh environments.

VSPP-Based Robotic Finger Design

A 3D model shows the construction of a robotic finger with two VSPP segments, presented in Figure 2A. The photo of the real prototype with major dimensions is shown in Figure 2B. Each VSPP segment has two distinctive features. When subjected to external force, the VSPP can adjust its contact

stiffness (Fig. 2C) by passive particle jamming. Besides, the VSPP is able to endure punctures of sharp objects (Fig. 2D) as long as the particles would not fall out.

The basic VSPP structure includes three components. The first is an elastic membrane, which is used to enclose the particles inside and ensure the original phalange shape. Second, within the elastic membrane, it is fully filled with particles (solid glass beads with diameter 3 mm). Third, a connector (3D-printed PLA, connected to the chamber by HY-30 glue) is used to seal the particle inside the elastic chamber and connect to the pin joint. In this prototype, the elastic membrane is molded by silicone (Dragon skin 20) and the beads are glass beads at 3 mm diameter. Connectors are printed by 3D PLA. This basic VSPP structure will perform a jamming phenomenon, which is majorly decided by the chamber thickness. The thicker the chamber, the stronger the passive jamming. To enlarge the compliance, we can use a relatively thin chamber to cooperate with flexible back support. Under this condition, the jamming will obviously be enhanced compared with the VSPP itself, as depicted in Figure 2E and F.

VSPPs are modular components. They can be connected by different joints to make a finger mechanism. For example, the phalange 1 in Figure 2A is connected to a pin joint. Because the VSPP has no actuation and only occupies the phalange part, the design for the pin joint is highly flexible. Most of the actuators or actuation mean used in both rigid and soft robotic hands can be applied to drive the VSPP segments, such as motor-driven, soft actuator-driven, cable-driven, and SMA-driven.

Here we use a soft pneumatic actuator to drive the joint in the prototype design. The soft linear actuator is mounted between two sides of the pin joints. By adjusting the pressure of soft actuator, the motion, open and close, of pin joint can be effectively controlled. The joint module is linked to another VSPP, illustrated as phalange 2 in Figure 2A. A flexible pipe embedded inside phalange 2 is used to provide compressed air to drive the joint. The joint can be easily modified to cable-driven actuation. Finally, the 2-segment VSPP can be mounted to a finger base or connected to more VSPP segments depending on the kinematics of the intended robotic hand.

The detail design process, component fabrication, and the versatile combination of VSPP to different actuations are illustrated in Appendix Figures A1 and A2, which provide specific guidance to replicate and apply VSPP in a customizable soft robot application.

VSPP Modeling

The modeling of VSPP is conducted from two perspectives. The first perspective focuses on the bending stiffness, which shows that the combination of the particle chamber and the flexible support layer creates synergy, enhancing the phalange/link stiffness. The second perspective is an analysis that the contact stiffness of VSPP resulted from the elastic pressure of the particle chamber under deformation.

VSPP bending stiffness modeling

The model to study VSPP bending stiffness is depicted in Figure 3, with related parameters listed in Table 2. Suppose a single-particle chamber (Fig. 3A), a single support layer (Fig. 3B), and a VSPP (Fig. 3C) are deformed to the same

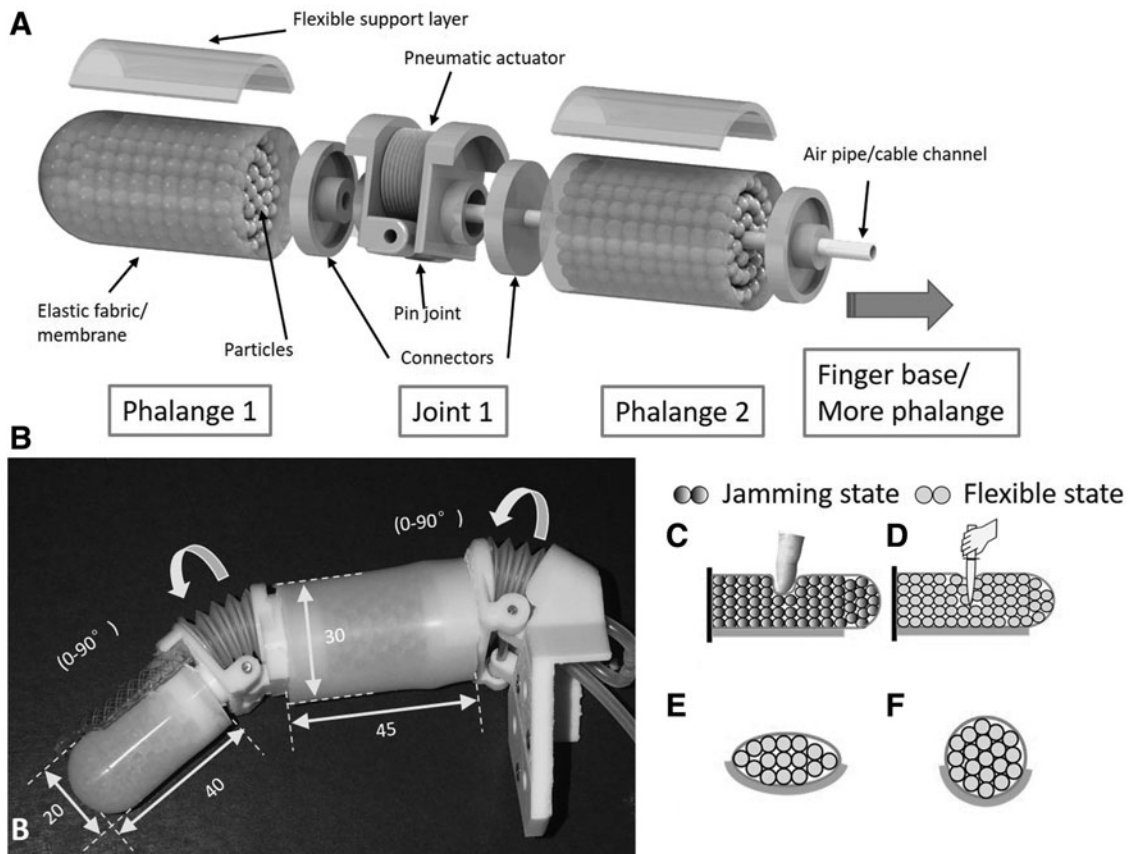


FIG. 2. Design of VSPP. (A) Finger with two VSPP segments. (B) The physic prototype of the VSPP-based finger. (C) VSPP stiffens under external load. (D) VSPP endures puncture. (E) Cross-sectional view of VSPP in circular shape with beam support. (F) Circular shape with arc support.

deflection Δ_d , the relevant push force for each is F_p , F_s , and F_m , respectively.

For the VSPP, the interacting force between the particle chamber and support layer is depicted in Figure 3D and E. The particle chamber functions as a medium that transforms the concentrated force F_m to a uniformly distributed load q by particle force chain (the particle chamber is assumed to conform to the support layer surface evenly).

We simplify the structure of the support layer as a cantilever beam to study its deflection. The deflection of a cantilever beam under concentration force F_s can be expressed as follows³⁵:

$$\Delta_d = \frac{F_s a^2}{6EI} (3L - a) \quad (1)$$

The deflection of a cantilever beam under distributed load q can be expressed as follows:

$$\Delta_d = \frac{qL^4}{8EI} \quad (2)$$

where E is the elastic modulus of the material, I is the moment of inertia, E and I are dependent on the material and thickness δ of the support layer, L is the overall length of the support

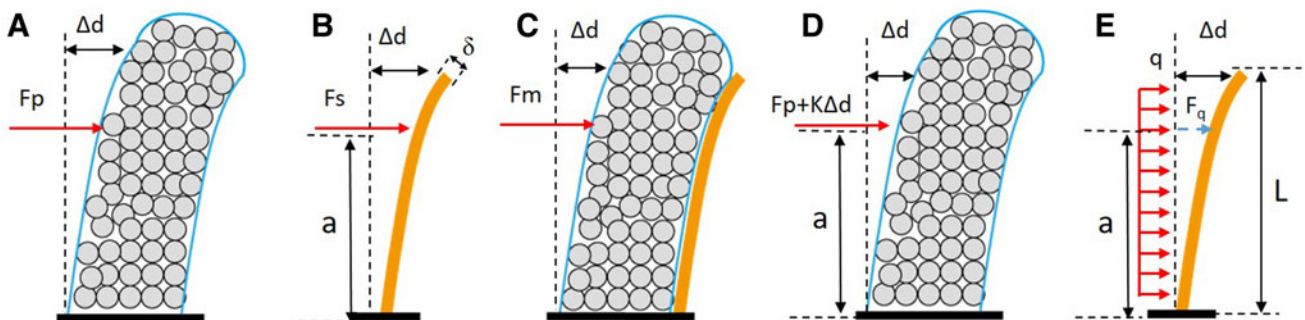


FIG. 3. Analytical modeling of VSPP bending stiffness. (A) Single-particle chamber bending. (B) Single flexible support layer bending. (C) VSPP overall bending. (D) Force analysis of particle chamber in VSPP overall bending. (E) Force analysis of flexible support layer in VSPP overall bending. Color images are available online.

TABLE 2. NOMENCLATURE OF THE VARIABLE STIFFNESS PARTICLE PHALANGE MODEL

Nomenclature of the VSPP model in Figure 3

Δ_d	Deflection constant
F_p	Force required for particle chamber to deflect at Δ_d
F_s	Force required for flexible support to deflect at Δ_d
F_m	Force required for VSPP to deflect at Δ_d
q	The distributive load transmitted from the particle chamber
F_q	Equivalent concentric force achieving the same deflection as caused by distributive load q
a	The position of force interaction point
L	Length of flexible support layer
δ	Thickness of flexible support layer
K	Particle jamming stiffness/contact stiffness

Nomenclature of the VSPP model in Figure 4

F	The interaction force of VSPP
Δ_s	Interaction deformation distance
P_{ela}	Pressure caused by chamber deformation
P_{pre}	Pressure caused by interactive force
L_0	VSPP original length
Δ_L	VSPP deformation length
h	VSPP original height
R_p	Deformation area ratio
Z	Studied jamming region height
Δ_Z	Studied jamming region height variation
Δ_Y	Studied jamming region ratio variation
F_{N1}	Normal force component in lateral view
F_{N2}	Normal force component in lateral view
F_{N3}	Normal force component in top view
F_{N4}	Normal force component in top view
f_{N1}	Friction component in lateral view
f_{N2}	Friction component in lateral view
f_{N3}	Friction component in top view
f_{N4}	Friction component in top view

VSPP, variable stiffness particle phalange.

layer, and a is the distance of the force interaction point from the base.

For the single support layer deflection under concentrated force F_s , the concentrated interaction force F_s and the deflection Δ_d are related by the following:

$$F_s = \frac{6EI\Delta_d}{a^2(3L-a)} \quad (3)$$

For the single support layer deflection under distributive load q , to achieve the same deflection Δ_d , the equivalent force F_q ($F_q = qL$) can be calculated by Equations (1) and (2):

$$F_q = \frac{4a^2(3L-a)}{3L^3} F_s \quad (4)$$

F_q is obviously larger than F_s . Thus, with the force transmission from concentrated force to distributive load, the required force to achieve the same deflection is increased. As a result, the bending stiffness of the flexible beam is increased. For example, when $a = L$, F_q is $\frac{8}{3}$ times of F_s .

For the whole VSPP structure, the bending stiffness is the combination of the flexible beam and particle chamber. The

force required to bend the particle chamber in VSPP is $F_p + K\Delta_d$, where $K\Delta_d$ is the stiffness enhanced by particle jamming in the VSPP structure; K is analyzed in the VSPP Contact Stiffness Modeling section.

$$F_m = F_q + F_p + K\Delta_d \quad (5)$$

Set $\alpha = F_p + F_s$ as the direct summation of bending force for particle chamber and bending support individually. The bending force difference between the VSPP structure (F_m) and the individual summation of forces in the particle chamber and the support layer (α) is as follows:

$$F_m - \alpha = F_q + F_p + K\Delta_d - F_s - F_p = F_q - F_s + K\Delta_d, \quad (6)$$

$$(0 \leq a \leq L)$$

which bending stiffness is further enlarged, with the particle jamming stiffness $K\Delta_d$, compared with flexible beam individually, as discussed in Equation (3). Thus, VSPP bending stiffness is structurally enhanced by the combination of particle chamber and a flexible layer, which means the overall bending stiffness is larger than that of the sum of particle chamber and support layer individually.

VSPP contact stiffness modeling

Following the bending stiffness analysis, an analytical model is built to study the contact stiffness of VSPP. We define the contact stiffness K as follows:

$$K = \frac{\Delta F_{vspp}}{\Delta_s} \quad (7)$$

where F is the interaction force and Δ_s is the deformation distance of VSPP as shown in Figure 3A. To simplify the model, here we omit the deformation of the interacting object and deflection of VSPP.

The reason for jamming is the elastic pressure induced by the passive deformation, which resulted from the interactive force. From the elastic mechanics for the elastic chamber, there is a relationship between elastic material expansion and its elastic pressure derived from the conservation of Helmholtz free energy³⁶⁻³⁸:

$$P_{ela}dV = \sigma dA \quad (8)$$

where V is the effective volume of an elastic membrane, A is the effective inner surface area of the elastic membrane, and P_{ela} is the inner pressure resulted from chamber material deformation. σ is the surface energy or surface tension, which is described as follows^{34,35}:

$$\sigma = \frac{S_+}{2} d_0 \left[1 - \left(\frac{r_0}{r} \right)^6 \right] \left[1 - \frac{S_-}{S_+} \left(\frac{r}{r_0} \right)^2 \right] \quad (9)$$

Thus, the elastic force resulted from the interactive force is

$$P_{ela} = \sigma \frac{dA}{dV} \quad (10)$$

Then, we consider the particles under the pressed region to study the contact stiffness. We simplify the regional particle

model as a cylindrical structure, as shown in Figure 4B. We assume the top and bottom of this cylinder, with radius R_p , have no deformation. The lateral side of this cylinder is covered by an elastic membrane. After compression, the top layer is pressed down and the lateral membrane is expanded, as illustrated in Figure 4C. The pressure in the chamber is the elastic pressure P_{ela} caused by the interaction force. During the deformation process, the force chain and friction between particles result in the jamming phenomenon and the resultant friction work is equal to the work caused by P_{ela} . We express this work conservation as follows:

$$F\Delta_z = W_{f\perp} + W_{fP}, \quad (11)$$

where Δ_z is the compressed deformation in Z direction, Δ_y is the expanded deformation in Y direction [$\Delta_y = \pi R_p \Delta_z / 2(h - \Delta_z)$ based on volume constant], $W_{f\perp}$ is the resultant friction work of particles in vertical direction, and W_{fP} is the resultant friction work in horizontal direction.

To get the resultant work, we first study the work and force of a single particle, as depicted in Figure 4C. The normal diameter of the particle is expressed as ϕ and the effective contact area is assumed at $A_{pre} = \pi\phi^2/4$.¹⁴ In the vertical direction, as depicted in Figure 4D, the value of friction is expressed as $f_{N2} = \mu F_{N2}$. The normal force F_{N2} is equal to $\frac{\sqrt{3}}{3} F_{N1} = \frac{\sqrt{3}}{3} (P_{ela}) A_{pre}$ based on force transmission.^{14,39} The friction coefficient is μ . In the vertical direction, the particle number is around $m = h\pi R_p^2 / \frac{4}{3}\pi\phi^3$. The displacement of each particle is $d\Delta_z$, which is the overall displacement dividing

the layers in the vertical direction, $\Delta_z / \left(\frac{h}{2\phi}\right)$. Thus, we can express the resultant particle friction work in the vertical direction as follows:

$$W_{f\perp} = \sum w_{f\perp} = mw_{f\perp} = 4mf_{N2}d\Delta_z \cos 30^\circ = 3\mu\pi R_p^2 \Delta_z P_{ela} / 4 \quad (12)$$

Similarly, in the horizontal direction, as depicted in Figure 4E, the horizontal work can be calculated. The normal force F_{N4} is equal to $\frac{\sqrt{3}}{3} F_{N3} = \frac{\sqrt{3}}{3} P_{ela} A_{pre}$ based on force transmission. The displacement of each particle is $d\Delta_y$, which is $\Delta_y / (2R_p / \phi)$. Thus, the friction work of particle can be calculated as follows:

$$W_{fP} = \sum w_{fP} = mw_{fP} = 4mf_{N4}d\Delta_y \cos 30^\circ = 3\mu\pi R_p h \Delta_y P_{ela} / 8 \quad (13)$$

By rearranging Equations (1), (6)–(12), and applying ($\Delta_s = \Delta_z$), we can express the interaction stiffness of VSPP, K_{vspp} , as a function of Δ_s as follows:

$$K = \frac{W_{f\perp} + W_{fP}}{\Delta_s^2} = \left(\frac{3\mu\pi R_p^2 \Delta_s}{4} + \frac{3\mu\pi^2 R_p^2 h \Delta_s}{16(h - \Delta_s)} \right) \frac{\sigma dA}{\Delta_s^2 dV} \quad (14)$$

The K can be calculated from Equations (7) and (14). From the modeling result, the design parameters' influence on VSPP segment contact stiffness can be predicted, as illustrated in Table 3.

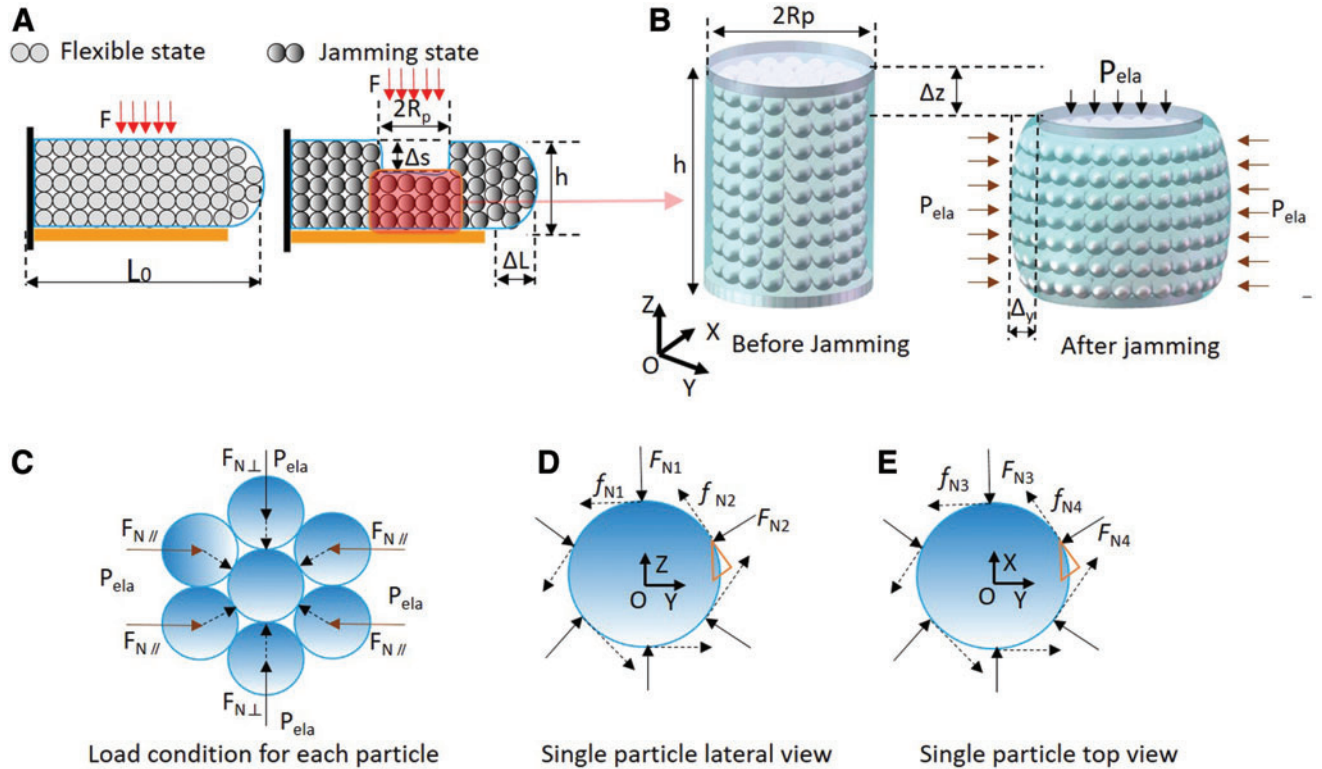


FIG. 4. Analytical modeling of VSPP contact stiffness. (A) Particles dislocate in VSPP at an outer force resulting in jamming. (B) The original state of the regional particle under interaction force and jammed state of a sample model to study the jamming process. (C) Force balance and distribution under jamming state for small regional particles. (D) Front view of a single particle under jamming state. (E) Top view of a single particle under jamming state. Color images are available online.

TABLE 3. DESIGN PARAMETER PREDICTION BASED ON VARIABLE STIFFNESS PARTICLE PHALANGE MODEL

Design parameter	Prototype parameter	Parameter influence on VSPP
Flexible support thickness: δ	2, 3 mm with 80 A	The thicker the flexible support, the larger the bending stiffness under the same interaction force.
VSPP chamber thickness: d_0	0.4, 0.8, 1.2, 2.0, 3.0 mm	The thicker the VSPP chamber, the larger the contact stiffness under the same interaction force.
Contact area: R_p	0.5, 4, 8, 16 mm	The larger the contact area, the larger the contact stiffness under the same interaction force.
Infilling particle size: Φ	2, 3, 4 mm	Particle size has a limited influence on VSPP jamming.
Chamber hardness: σ	40 A, 50 A, 60 A	The harder the VSPP chamber, the larger the contact stiffness under the same interaction force.

Experimental Validation

The experimental validation consists of two perspectives. The first section experiments the variable stiffness performance of the VSPP segment, including both bending stiffness and contact stiffness validation; the second part tests the performance of prototype finger constructed by VSPP segments, including tests on grasping robustness and lateral compliance.

VSPP segment validation

Altogether, five groups of experiments are designed to validate the characteristic of the prototype VSPP segments. The first two groups are used to study the bending stiffness enhanced by the flexible support layer. The other three tests are dedicated to the contact stiffness of VSPP. The influence of three major design parameters is studied, which include membrane thickness, particle size, and the VSPP interaction area.

The test platform is presented in Figure 5A. Two blocks on the linear guides are connected in series. A force gauge is mounted on the left block and the test VSPP prototype is mounted on the right one. A test probe with a 4-mm-diameter head is mounted on the force gauge. By moving the test probe head on the force gauge to push the VSPP prototype, a force can be measured. We set the initial contact point (contact force 0.1 N) as the start point. The test will stop when the displacement reaches 10 mm, or the pushing force reaches 20 N (protect test equipment), whichever is first. The real-time interaction force is recorded by computer from the force gauge reading, and each test is repeated 10 times to take the average value. The customized VSPP segments are depicted in Figure 5B.

The first group of the experiment is intended to validate the bending stiffness enhancement resulted from the combination of particle chamber and flexible support layer. Three experiments are conducted: (1) only the particle chamber (glass particle at size $\Phi=3$ and membrane with thickness $\delta=1.2$), (2) the particle chamber supported by a flexible arch layer (2 mm thickness hybrid nylon layer with hardness 80 A), this is the proposed VSPP, (3) and the flexible support layer only (2 mm thickness hybrid nylon layer with hardness 80 A). All the experiments were conducted using a probe head at 8.00 diameter (M8), as shown in Figure 5C. The interaction point is at the middle point of VSPP segment. The results are presented in Figure 6A. It can be seen that the interaction force of VSPP is around two times the sum from the particle chamber only and support layer only. This result is consistent with the bending model derived in the VSPP Bending Stiffness Modeling section. The results prove that the combination of flexible support layer and compliant particle chamber results in enhanced bending stiffness as analyzed in the VSPP Bending Stiffness Modeling section.

The second test is applied to compare the influence of flexible layer bending stiffness on VSPP bending stiffness. Three experiments are conducted: (1) the particle chamber supported by a flexible layer (2 mm thickness hybrid nylon layer with hardness 80 A), (2) the particle chamber supported by a flexible layer (3 mm thickness 3D-printed TPU layer with hardness 80 A), and (3) the particle chamber supported by a rigid support layer (3 mm thickness 3D-printed PLA support). All the experiments conducted using a probe head at 8.00 diameter (M8) are shown in Figure 5C. The interaction point is at the middle point of the VSPP segment. Results are presented in Figure 6B, which shows that the thicker/harder the support layer, the larger the bending stiffness of the VSPP. Thus, the bending stiffness of VSPP is easily customized by choosing suitable stiffness support layers.

The remaining three tests are processed on the rigid support layer to study the maximum contact stiffness of VSPP, as shown in Figure 5F.

The third test studies the particle size influence on contact stiffness. Keeping other parameters the same ($d_0=2.0$), three VSPP prototypes with particle size Φ at 3, 4, and 5 mm are compared. The result in Figure 5C shows that particle size has a limited influence on jamming performance. This is also in accordance with the contact stiffness modeling result, which proves that the particle size is not a major factor having an influence on VSPP stiffness performance.

The fourth test validates the VSPP's contact stiffness behavior at different elastic membrane thicknesses. In these tests, five VSPP prototypes with rubber membrane thickness d_0 at 0.4, 0.8, 1.2, 2.0, and 3.0 mm are prepared (all have the same particle size $\Phi=3$, a circular cross section with $L_0=45$ mm, and $h=20$ mm). The test head probe is M8 in all the pushing tests at the middle point of VSPP segments. The results are presented in Figure 6D. The result shows that the thicker the membrane, the larger the interaction force will be, which is constant with modeling prediction. This phenomenon can be explained by the fact that a thicker membrane provides a larger elastic pressure P_{ela} under the same particle chamber volume change, thus results in a stronger passive particle jamming.

The fifth group of experiment studies the influence of the interaction area on the VSPP jamming effect. Four test probe

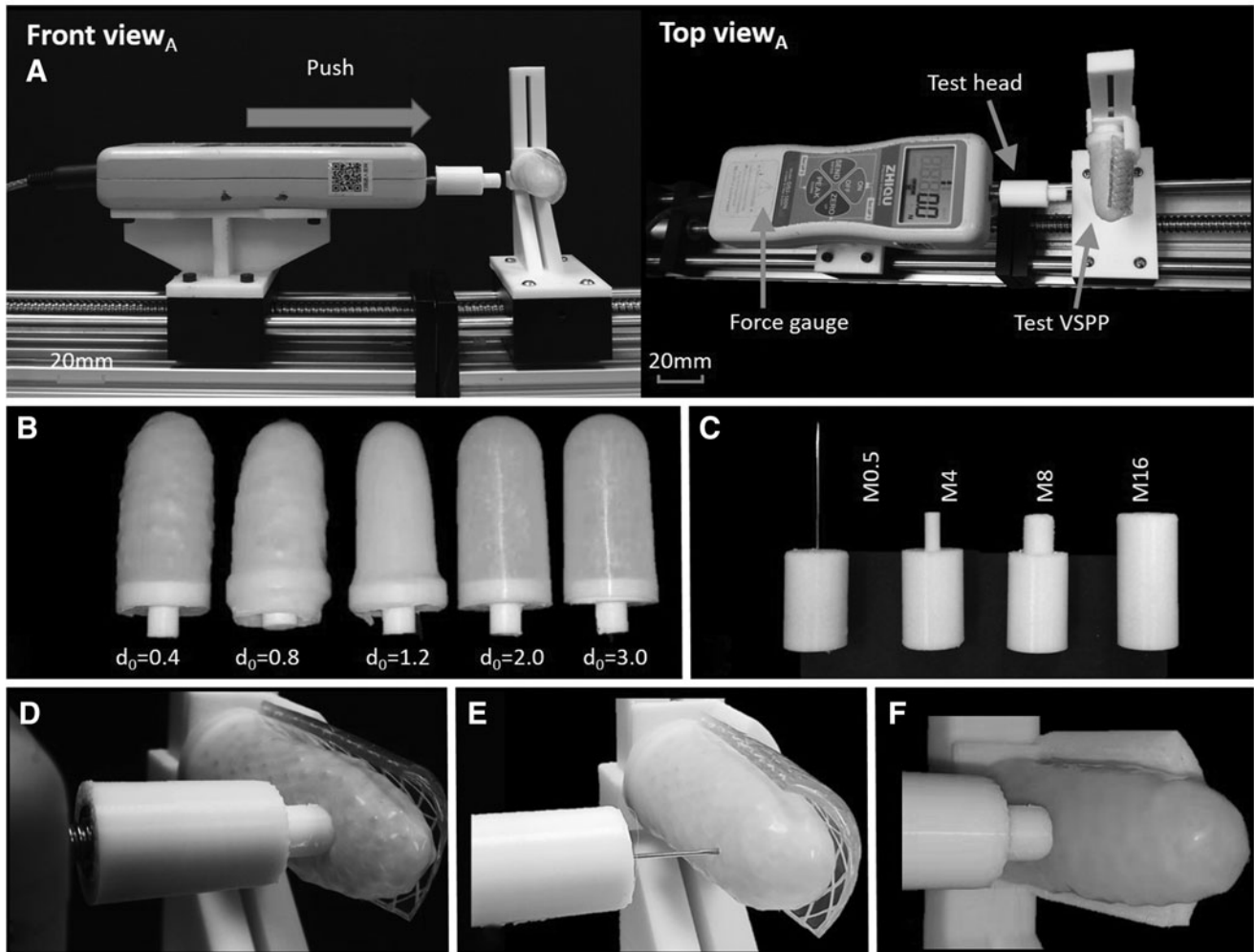


FIG. 5. Experimental platform setup and tests of prototype VSPP segments. (A) Test platform for studying the VSPP design parameter influence. (B) Fabricated VSPP prototypes with different chamber thicknesses. (C) Four kinds of dedicated test heads. (D) Jamming state of VSPP segment. (E) Pierced state of VSPP segment. (F) Rigid support to study the maximum contact stiffness of VSPP.

head diameters: 0.5 (needle), M4, M8, and M16 respectively, as shown in Figure 5C, are used for the tests. The test result is presented in Figure 6E. It shows that the larger the interaction area, the larger the interaction force created by the VSPP. The result is consistent with modeling prediction. The larger the interaction area, the larger the deformation of the elastic chamber will be, which results in larger P_{ela} providing stronger jamming between particles.

Furthermore, the punctation test of VSPP is processed as depicted in Figure 5E. This experiment is processed by repeatedly puncturing the VSPP prototypes 30 times at random locations. After multiple punctuations, the VSPP prototype still remains effective to provide contact stiffness and interaction force. This presents excellent application durability.

With the above data, we can compare the results of the experiments with analytical modeling. From the experimental result, we pick out the test data of the VSPP prototype with particle size $\Phi = 3$ mm, chamber membrane thickness $d_0 = 1.2$ mm, chamber length $L_0 = 35$ mm, and chamber height $h = 20$ mm under the interaction with an M8 probe head. By referring to the material table, the parameters for calculating σ are $u = 0.4$, $S_+ = 150$ kPa, and $S_- = -15$ kPa. Then, we input

these data to our analytical contact stiffness K_{vspp} expression in Equations (7) and (14), and the stiffness at a given displacement could be calculated. The result comparison is shown in Figure 6F. Both results show that the interaction stiffness increases when the interacting deformation enlarges. The experimental result is generally in accordance with the analytical result within 3 mm deformation. A discrepancy between the theoretic calculation and experiments is noticed under deformation larger than 3 mm. This discrepancy might be explained that the model just considers the elastic pressure caused by chamber deformation. Under small deformation, the influence of the support layer is not so obvious; under large deformation, the support layer influence is obvious and provides a further interaction force. Overall, the proposed analytical model can be used to explain the VSPP jamming mechanism and guide the VSPP design, as discussed in Table 3.

VSPP-based robotic finger validation

The fifth and sixth groups of experiments compare the compliance of three-finger prototypes, depicted in Figure 7A.

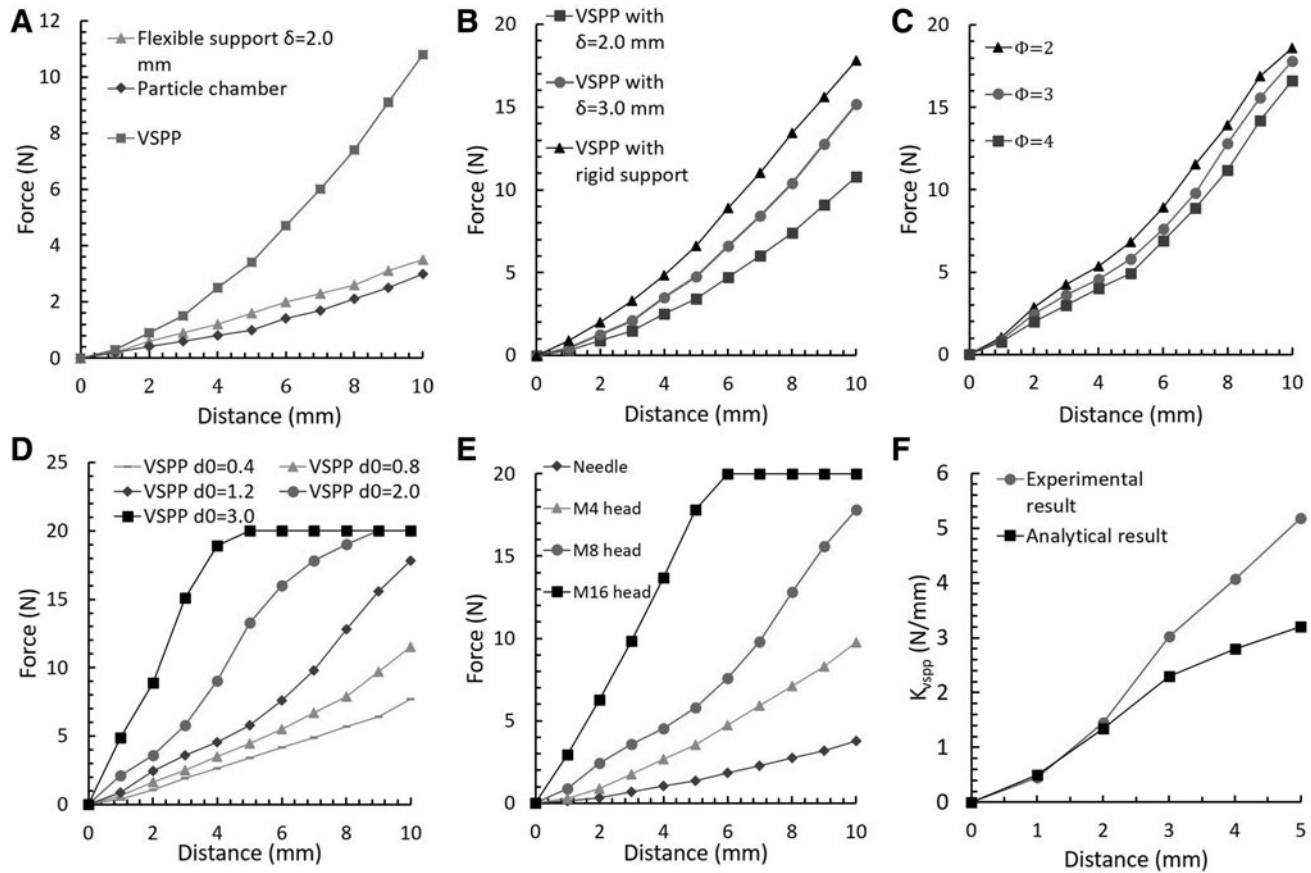


FIG. 6. Experimental validation of VSPP segments. (A) Support layer enhancement of bending stiffness. (B) Support layer stiffness influence on bending stiffness. (C) Particle size influence on contact stiffness. (D) VSPP chamber thickness influence on contact stiffness. (E) Interaction area influence on contact stiffness. (F) Analytical and experimental results of contact stiffness comparison.

The VSPP finger design parameters are particle size $\Phi=3$ mm, membrane thickness $d_0=2.0$ mm, $L_0=35$ mm, and $h=20$ mm for the distal phalange, and particle size $\Phi=3$ mm, chamber membrane thickness $d_0=3.0$ mm, $L_0=40$ mm, and $h=30$ mm for the proximal phalange. All fingers share the same design except the material of the phalanges. The rigid finger prototypes (Finger#1 in Fig. 7D) have all PLA-printed rigid phalange (covered with a layer of silicone at 2 mm thickness as a usually applied approach to enhance contact friction), and the soft finger uses silicone rubber (Dragon skin 30)-molded solid distal phalange. The whole finger dimension has been depicted previously in Figure 2B.

The comparison is made in two aspects, the lateral compliance and the grasping robustness. For the lateral compliance comparison test, as shown in Figure 4E, the force gauge is mounted on a vertical slideway and the finger prototype is mounted on a horizontal slideway. We move the horizontal slideway toward the M4 probe head on the force gauge against the side surface of the test finger. The lateral pushing distance is also 10 mm, or pushing force 20 N, whichever is reached first. We repeat the test for each finger 20 times and take the averaged data. The test result is shown in Figure 7E. As can be seen, the soft phalange finger provides the largest lateral compliance. The rigid phalange finger provides the least lateral compliance. A too-small compliance lacks enough structural rigidity for reliable grasping and the lack of

compliance results in poor human/robot interaction safety. For the proposed VSPP finger, its lateral compliance is in-between the soft and rigid phalange fingers. By adjusting design parameters, in fact, the lateral compliance of VSPP has a large modulation range, which can be customized to specific working requirements. By this means, the VSPP finger can be designed with the required lateral compliance, to provide both reliable grasping capability and safe human/robot interaction.

The last group of experiments compares the grasping robustness of the three dedicated fingers. Four test surfaces are selected for this comparison, as shown in Figure 7C, which includes #1 spiky surface (mimics the surface of spiky objects such as the durian, the spiky feature is with 1.5 mm distal diameter), #2 arc surface, #3 triangular surface, and #4 flat surface. The test process is depicted in Figure 7D with the test surface mounted at the end of a force gauge in left slideway and the finger prototype is mounted on the right slideway. We input 100 kPa pressure into the pneumatic actuator of each joint and let the distal phalange contact on the test surface. Then we control the motor of the left slideway to move the force gauge left. The maximum pulling force is recorded by the computer. Each pull out test is repeated 20 times and we take the averaged data. One additional test is done on the VSPP with a deliberately punctured membrane with 1.5 mm holes. Thus, four groups of results are presented in Figure 6F. It can be noticed that the VSPP finger performs better than a

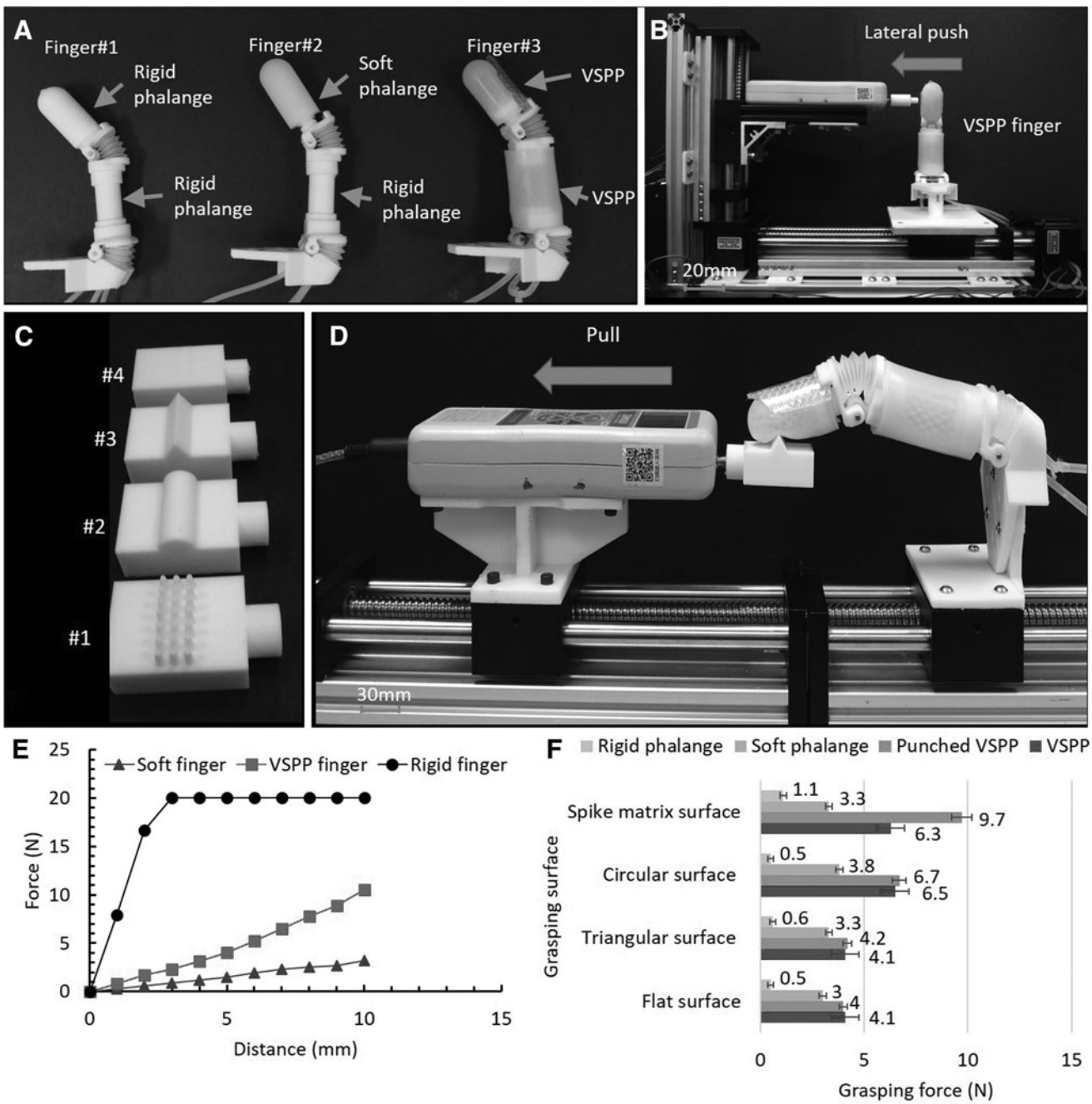
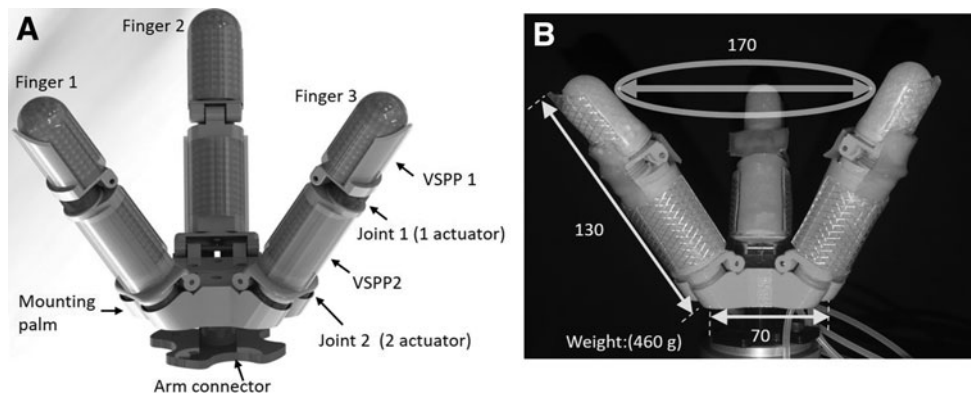


FIG. 7. Grasping robustness comparison. (A) Three kinds of prototype fingers with different phalanges. (B) Lateral compliance test setup. (C) Four dedicated test surfaces with spiky surface, circular surface, triangular surface, and flat surface. (D) Grasping robustness test setup. (E) The lateral compliance comparison result. (F) The grasping robustness comparison result.

FIG. 8. The prototype gripper VSPP-3. (A) A 3D model showing major components of the gripper. Each finger has two VSPPs and two joints. (B) A prototype of VSPP-3 with overall dimensions. 3D, three-dimensional.



rigid and soft phalange finger toward all four types of test surfaces, and the superiority is more marked for a spiky surface. This can be explained by the excellent adaptability of VSPP finger and variable stiffness feature. Although the soft phalange finger also shows good adaptability, it lacks structural rigidity under large deformation. For the rigid phalange finger, although covered by a layer of silicone to enhance friction, the insufficient adaptability limits its grasping performance. Turn to the punctured VSPP finger, it performs similarly to the unpunctured VSPP finger on surface type #2–4, but performs strikingly better on the spiked surface. This

may be explained by the porous membrane of VSPP providing a larger contact area when interacting with spiky surfaces. Thus, the porous membrane can be regarded as an enhanced VSPP design selection, which can be achieved using porous fabric to enclose the particles or deliberately perforating the silicone rubber membrane.

Overall, the basic stiffness of VSPP ranges from 0 to 7 N/mm in our different VSPP prototypes, which is highly customizable based on the design parameter selection. The stiffness variation ratio of one VSPP is up to five times under 10 mm deformation compared with a 1 mm deformation.

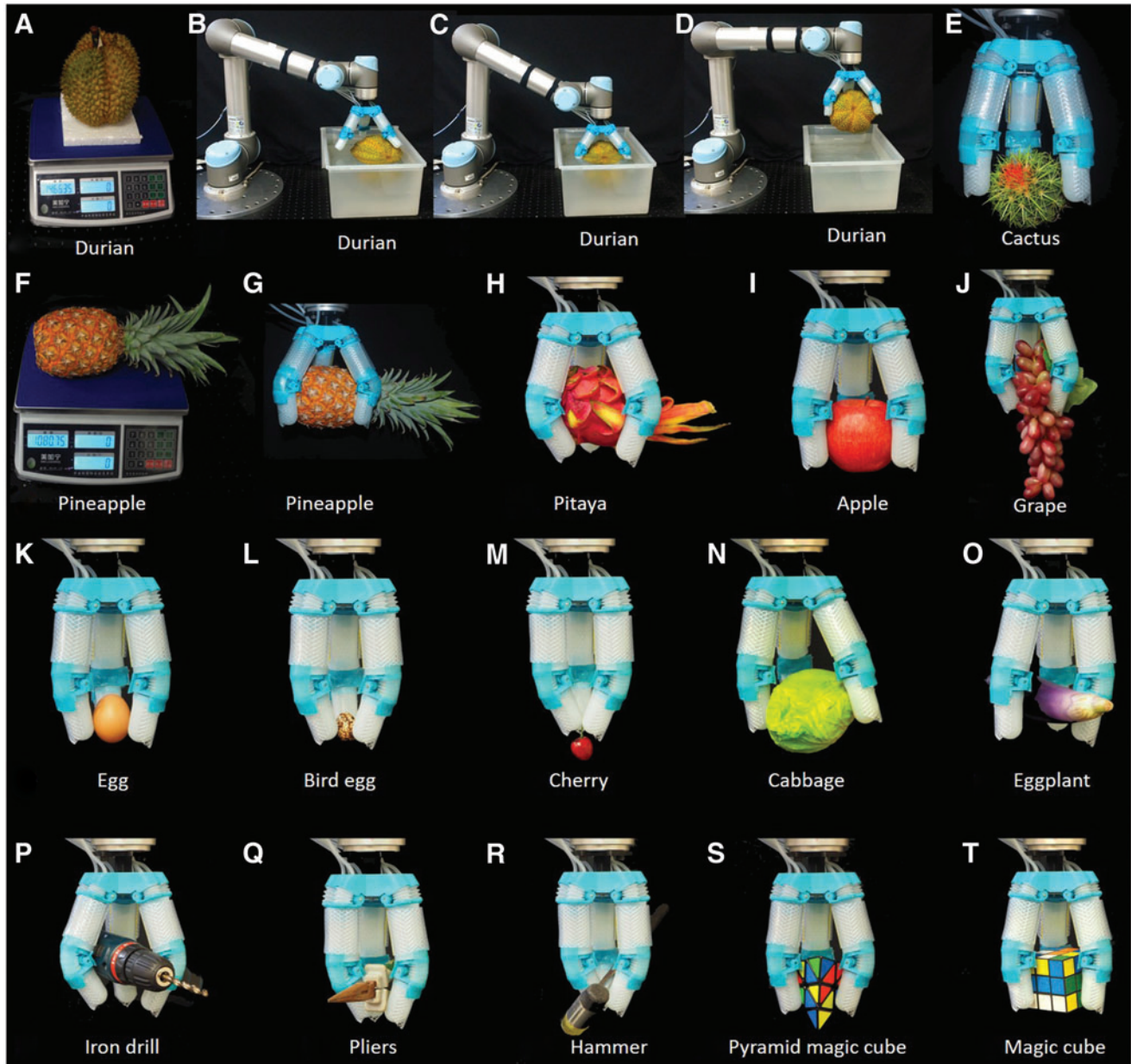


FIG. 9. VSPP-3 gripper grasping performance and grasping system realization. (A) VSPP-3 successfully grasping a durian, which is about 1.5 kg and with spinous features, and (B–D) grasping durian out from the water. (E) VSPP-3 successfully grasping a cactus with surface pierced by spines. (F, G) VSPP-3 successfully grasping a pineapple, which is about 1.1 kg with spinous features. VSPP-3 successfully grasping daily objects, including various objects with different softness, such as (H) a soft pitaya, (I) an apple, (J) a bunch of grapes, (K) a chicken egg, (L) a bird egg, (M) a cherry, (N) a cabbage, (O) an eggplant, (P) an iron drill, (Q) pliers, (R) a hammer, (S) a pyramid magic cube, and (T) a magic tube. Color images are available online.

Grasping robustness, processing durability, and interaction compliance are excellently demonstrated in the VSPP-based prototype.

Prototype Gripper Implementation and Performance Demonstration

Following the systematic study on the proposed VSPP segment, we build a three-fingered gripper called VSPP-3 based on VSPP to demonstrate the superior grasping capability and robustness. For each finger, we use the same design parameters as the prototype VSPP finger used in the above experimental validation. The three fingers of VSPP-3 are uniformly distributed with 120° between each other. A rendered 3D computer model is shown in Figure 8A to show all major components in the gripper design. A prototype of the model showing the major dimensions is shown in Figure 8B. The weight of the prototype VSPP-3 is only about 460 g.

For grasping the demonstration, we mount the VSPP-3 gripper at the end of a UR5 manipulator. The grasping performance of VSPP-3 is demonstrated by grasping of selected daily objects, they are either great challenges for traditional soft grippers due to their sharp spiky surface (durian, cactus, etc.) and weight (durian), or difficult to handle by rigid grippers due to their vulnerability (grape, egg, etc.).⁴⁰ As we anticipated, the VSPP-3 gripper adapts excellently for all these objects, including spiky surface, such as the durian, cactus, and pineapples, as shown in Figure 9A–T. Safe grasping of thorny objects is a challenge for both soft and rigid grippers. For rigid gripper, the rigid contact easily results in damage to the spiky feature and grasping instability because of the small contact area between the gripper and the spikes. Inversely, soft grippers are easily pierced by sharp spikes, resulting in their functional failure, or grasping efficacy. Besides, the heavyweight of those spiky fruits is also a challenge for the existing soft grippers. However, the VSPP-based gripper offers great potential toward the above problems. Furthermore, the grasping effectiveness of the VSPP gripper is reliable even in underwater conditions. We present the underwater durian grasping as depicted in Figure 9B–D, the VSPP still functions properly even though pieced by durian spikes because VSPP does not need to be air- or water-tight. Thus, compared with the traditional soft grippers, the VSPP-based gripper is more reliable and endurable in a harsh working environment. For example, grasping a spiky creature in deep sea, which is a challenge for a traditional pneumatic soft gripper, is fully realizable for the VSPP gripper.

Other daily objects with different characteristics that range from small delicate objects, such as a cherry and bird egg, to a relatively large and heavy object, such as a power drill and hammer, are successfully and reliably grasped by the VSPP-3. A video file showing all the dynamic grasping demonstrations is submitted as a supplementary file together with this article.

Conclusion

Traditionally, robotic grippers have either rigid or soft phalanges. Grippers with rigid phalanges, usually with pin joint mechanisms, have very good grasping robustness and processing durability. Grippers with soft material phalanges, normally actuated by pneumatic power, represent more recent research, having superior performance in adaptability and safe human/robot interaction. These two types of grippers represent

two extreme application scenarios. When accuracy and high payload are required, rigid robot grippers are the obvious choice. In handling delicate objects (normally light) or in human/robot interaction, soft grippers are the preferred choice.

In this article, we have presented a bridge or a complementary approach to robotic grippers. Instead of studying the actuation methods, we have focused on an essential part of a robotic finger, the phalange. We proposed a novel VSPP to build robotic grippers. It has been shown with the merits of both soft and rigid end-effectors. The VSPP exhibits variable stiffness feature, resulted from passive particle jamming, under different grasping forces. The VSPP can cooperate with many actuators, both soft and rigid, to achieve a compliant robotic finger. The finger based on VSPP is functional and reliable in air and water, even when pierced by sharp objects such as a needle, exhibiting excellent durability in a harsh environment. The inherent multidirectional compliance persisting in VSPP is a good feature for safe robot/human interaction. The VSPP-based robotic gripper has the characteristics of soft grippers in small contact/force interaction and presents the features of rigid robotic grippers under large contact/force interaction. This is a promising feature for the proposed VSPP to be used for more applications, or as a complementary solution to rigid or soft grippers.

The theoretic modeling of the proposed VSPP is also presented in detail in the article. The influence of major design parameters on VSPP performance is studied. Three-finger prototypes, one based on rigid phalange, another based on soft phalange, and the third based on VSPP, have been built for various performance comparison experiments. A three-fingered prototype gripper, VSPP-3, with a pneumatic actuator is built. The gripper has been shown with reliable grasping toward daily objects ranging from a soft delicate cherry to a large and heavy power drill. A special feature is its robustness and durability in handling objects with spiky surfaces, both in the air or underwater. This has been demonstrated in grasping thorny and heavy durian, cactus, and pineapple. This capability is unimaginable by the traditional soft grippers. Thus, robotic grippers/hands based on the proposed VSPP have great potential to more daily applications in the human environment.

Author Disclosure Statement

No competing financial interests exist.

Funding Information

This work was supported by Shenzhen/Hong Kong Innovation Circle Programme (Type D SGDX2019081623201196).

References

1. Rus D, Tolley MT. Design, fabrication and control of soft robots. *Nature* 2015;521:467–475.
2. Cho KJ, Koh JS, Kim S, *et al.* Review of manufacturing processes for soft biomimetic robots. *Int J Precis Eng Manuf* 2009;10:171–181.
3. Bicchi A. Hands for dexterous manipulation and robust grasping: A difficult road toward simplicity. *IEEE Transact Robot Autom* 2000;16:652–662.
4. Dollar AM, Howe RD. The highly adaptive SDM hand: Design and performance evaluation. *Int J Robot Res* 2010; 29:585–597.

5. Kim S, Laschi C, Trimmer B. Soft robotics: A bioinspired evolution in robotics. *Trends Biotechnol* 2013;31:287–294.
6. Polygerinos P, Correll N, Morin SA, *et al.* Soft robotics: Review of fluid-driven intrinsically soft devices; manufacturing, sensing, control, and applications in human-robot interaction. *Adv Eng Mater* 2017;19:1700016.
7. Polygerinos P, Wang Z, Overvelde JTB, *et al.* Modeling of soft fiber-reinforced bending actuators. *IEEE Transact Robot* 2015;31:778–789.
8. Galloway KC, Polygerinos P, Walsh CJ, *et al.* Mechanically programmable bend radius for fiber-reinforced soft actuators. In 2013 16th International Conference on Advanced Robotics (ICAR). Karlsruhe, Germany: IEEE, 2013:1–6.
9. Khatib O, Yeh X, Brantner G, *et al.* Ocean one: A robotic avatar for oceanic discovery. *IEEE Robot Autom Mag* 2016;23:20–29.
10. Li Y, Chen Y, Ren T, *et al.* Precharged pneumatic soft actuators and their applications to untethered soft robots. *Soft Robot* 2018;5:567–575.
11. Kim HI, Han MW, Song SH, *et al.* Soft morphing hand driven by SMA tendon wire. *Compos B Eng* 2016;105:138–148.
12. Yang Y, Chen Y, Li Y, *et al.* Bioinspired robotic fingers based on pneumatic actuator and 3D printing of smart material. *Soft Robot* 2017;4:147–162.
13. Yang Y, Chen Y, Li Y, *et al.* Novel variable-stiffness robotic fingers with built-in position feedback. *Soft Robot* 2017;4:338–352.
14. Li Y, Chen Y, Yang Y, *et al.* Passive particle jamming and its stiffening of soft robotic grippers. *IEEE Transact Robot* 2017;33:446–455.
15. Amend JR, Brown E, Rodenberg N, *et al.* A positive pressure universal gripper based on the jamming of granular material. *IEEE Transact Robot* 2012;28:341–350.
16. Guo J, Xiang C, Rossiter J. A soft and shape-adaptive electroadhesive composite gripper with proprioceptive and exteroceptive capabilities. *Mater Design* 2018;156:586–587.
17. Shian S, Bertoldi K, Clarke DR. Dielectric elastomer based “grippers” for soft robotics. *Adv Mater* 2015;27:6814–6819.
18. Araromi OA, Gavrilovich I, Shintake J, *et al.* Rollable multisegment dielectric elastomer minimum energy structures for a deployable microsatellite gripper. *IEEE ASME Transact Mechatron* 2014;20:438–446.
19. Wei Y, Chen Y, Ren T, *et al.* A novel, variable stiffness robotic gripper based on integrated soft actuating and particle jamming. *Soft Robot* 2016;3:134–143.
20. Zhou J, Chen S, Wang Z. A soft-robotic gripper with enhanced object adaptation and grasping reliability. *IEEE Robot Autom Lett* 2017;2:2287–2293.
21. Zhou J, Yi J, Chen X, *et al.* BCL-13: A 13-DOF soft robotic hand for dexterous grasping and in-hand manipulation. *IEEE Robot Autom Lett* 2018;3:3379–3386.
22. Zhou J, Chen X, Li J, *et al.* A soft robotic approach to robust and dexterous grasping. In 2018 IEEE International Conference on Soft Robotics (RoboSoft). Livorno, Italy: IEEE, 2018:412–417.
23. Zhang YF, Zhang N, Hingorani H, *et al.* Fast-response, stiffness-tunable soft actuator by hybrid multimaterial 3D printing. *Adv Funct Mater* 2019;29:1806698.
24. Hughes J, Culha U, Giardina F, *et al.* Soft manipulators and grippers: A review. *Front Robot AI* 2016;3:69.
25. Blanc L, Delchambre A, Lambert P. Flexible medical devices: Review of controllable stiffness solutions. *Actuators* 2017;6:23.
26. Vanderborght B, Albu-Schäffer A, Bicchi A, *et al.* Variable impedance actuators: A review. *Robot Autonom Syst* 2013;61:1601–1614.
27. Stilli A, Wurdemann HA, Althoefer K. A novel concept for safe, stiffness-controllable robot links. *Soft Robot* 2017;4:16–22.
28. Sadeghi A, Beccai L, Mazzolai B. Innovative soft robots based on electro-rheological fluids. In IEEE/RSJ International Conference on Intelligent Robots and Systems (IROS), Vilamoura, Portugal, 2012:4237–4242.
29. Majidi C, Wood RJ. Tunable elastic stiffness with microconfined magnetorheological domains at low magnetic field. *Appl Phys Lett* 2010;97:164104.
30. Williams KA, Chiu GTC, Bernhard RJ. Controlled continuous tuning of an adaptively tunable vibration absorber incorporating shape memory alloys. *Smart Structures and Materials 2000: Mathematics and Control in Smart Structures*. International Society for Optics and Photonics 2000; 3984:564–576.
31. Shintake J, Schubert B, Rosset S, *et al.* Variable stiffness actuator for soft robotics using dielectric elastomer and low-melting-point alloy. In RSJ International Conference on Intelligent Robots and Systems (IROS), IEEE, Hamburg, Germany, 2015:1097–1102.
32. Shan W, Diller S, Tutcuoglu A, *et al.* Rigiditytuning conductive elastomer. *Smart Mater Struct* 2015;24:065001.
33. Murray RM, Li Z, Sastry SS. *A Mathematical Introduction to Robotic Manipulation*. Boca Raton, FL: CRC Press, 1994.
34. de Payrebrune KM, O’Reilly OM. On constitutive relations for a rod-based model of a pneu-net bending actuator. *Extreme Mech Lett* 2016;8:38–46.
35. Boreni AP, Schmidt RJ, Sidebottom OM. *Advanced Mechanics of Materials*. Vol. 6. New York: Wiley, 1985.
36. Timoshenko SP, Gere JM. *Theory of Elastic Stability*. New York: McGraw-Hill, 1961.
37. Necas J, Hlaváček I. *Mathematical Theory of Elastic and Elasto-Plastic Bodies: An Introduction*. New York: Elsevier, 1981.
38. Müller I, Strehlow P. *Rubber and Rubber Balloons: Paradigms of Thermodynamics*. Berlin Heidelberg, Germany: Springer-Verlag, 2004.
39. Yang Y, Zhang Y, Kan Z, *et al.* Hybrid jamming for bioinspired soft robotic fingers. *Soft Robot* 2019. [Epub ahead of print]; DOI: 10.1089/soro.2019.0093.
40. Zhou J, Chen Y, Chen X, *et al.* A proprioceptive bellows (PB) actuator with position feedback and force estimation. *IEEE Robot Autom Lett* 2020;5:1867–1874.

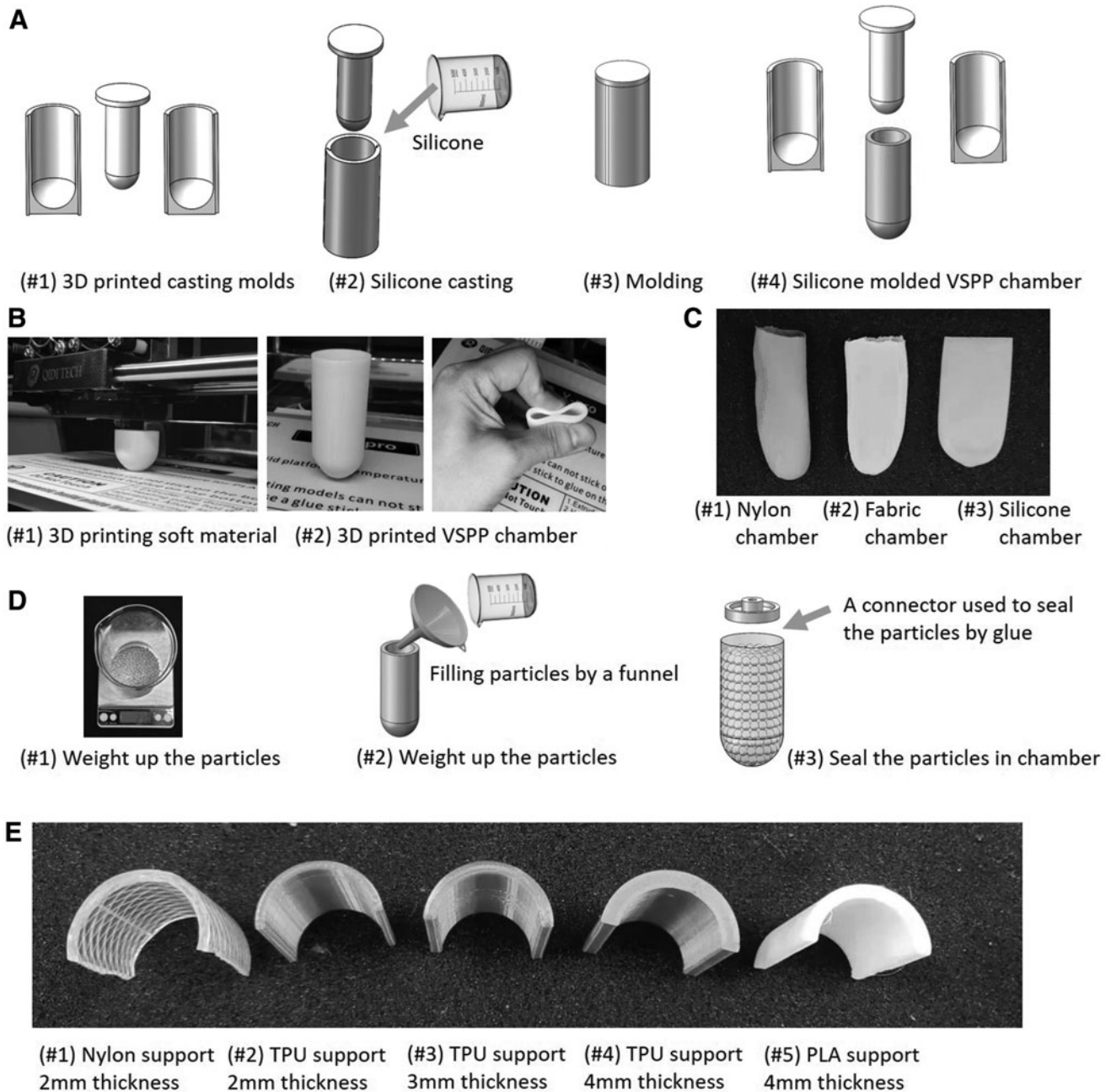
Address correspondence to:

Yonghua Chen
 Department of Mechanical Engineering
 The University of Hong Kong
 Pokfulam Road
 Hong Kong
 Hong Kong

E-mail: yhchen@hku.hk

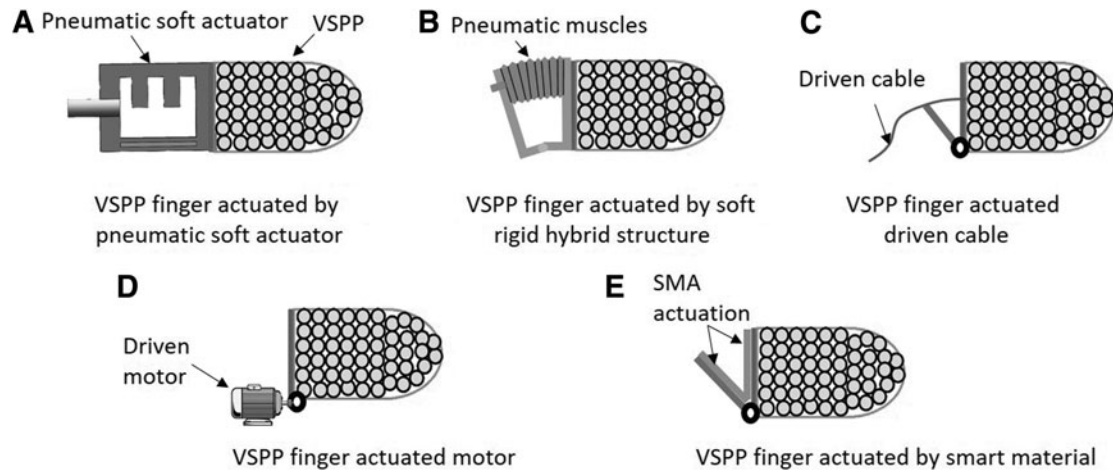
(Appendix follows →)

Appendix



APPENDIX FIG. A1. The simple fabrication process of VSPP. (A–C) Recommended fabrication approaches of VSPP chamber. (A) Molding and casting soft material approach. (#1) 3D-printed casting molds with one inner mold and two outer molds. (#2) Silicone casting in molds. (#3) Silicone molding. (#4) The modeled VSPP chamber. (B) 3D printing soft material approach. (#1–#2) 3D-printed VSPP chamber. (C) Commercially available elastic gloves or finger covers. (#1) Nylon chamber. (#2) Fabric chamber. (#3) Rubber chamber. (D) Particle filling process illustration. (#1) Weight up the particles based on estimation chamber size. (#2) Particle filling by a funnel with suitable in-hand vibration. (#3) Sealing particle in VSPP chamber by the connector with silicone glue (TY-340). (E) Customizable flexible support layer. (#1) Nylon support at 2 mm thickness. (#2) 3D-printed TPU support at 2 mm thickness. (#3) 3D-printed TPU support at 3 mm thickness. (#4) 3D-printed TPU support at 4 mm thickness. (#5) 3D-printed PLA support at 4 mm thickness. 3D, three-dimensional; VSPP, variable stiffness particle phalange.

(Appendix continues →)



APPENDIX FIG. A2. Potential actuation approaches for VSPP-based fingers. **(A)** Pneumatic soft actuator-actuated VSPP finger. **(B)** Soft/rigid hybrid structure of VSPP finger. **(C)** Cable-driven VSPP finger. **(D)** Motor-driven VSPP finger. **(E)** Smart material-actuated VSPP finger.